A Multi-Objective Real-Time Trajectory Planning Framework for Human–Machine Mixed Traffic Based on Self-Attention Guided CNN-LSTM

Gaochang Zhang, Zhida Xing, Yue Qiu, Runjiao Bao, Kun Liu, *Senior Member, IEEE*, Yuanqing Xia, *Fellow, IEEE*, and Senchun Chai, *Senior Member, IEEE*

***Abstract*— Human-machine mixed traffic (HMMT) where autonomous ground vehicles (AGVs) coexist with human-driven vehicles (HDVs), is expected to be the predominant transportation mode in the foreseeable future. To address the multi-objective real-time lane-change trajectory planning problem for AGVs in HMMT, this study proposes a self-attention guided convolutional neural network-long short-term memory network (CNN-LSTM) based framework. This framework introduces an interval type-2 fuzzy physical programming (IT2FPP) method to iteratively solve the trajectory planning problem under varying HDV driving intentions and constructs a dataset using the corresponding HMMT system states and AGV control actions. IT2FPP can handle uncertainties in all boundaries of the preference function and accommodate fuzzy preferences from multiple decision-makers, overcoming the limitations of type-1 fuzzy physical programming. Additionally, a fitting function-based obstacle avoidance method is proposed to model obstacles in the trajectory planning problem with fitting functions, ensuring collision-free trajectories while improving computational efficiency. Then, a self-attention guided CNN-LSTM network is designed to learn the mapping function between the HMMT system states and AGV control actions, enabling real-time trajectory planning with very low computational burden. The network effectively extracts intrinsic features from time series data, demonstrating high accuracy. As HDV driving intentions are incorporated in the dataset, there is no need for inference when generating AGV trajectories in real-time, further enhancing planning efficiency. The framework effectively addresses the multi-objective real-time lane-change trajectory planning problem for AGVs in HMMT, demonstrating high accuracy, real-time performance, and practical application potential, as validated by simulation and physical experiments.**

***Index Terms*— Neural network, interval type-2 fuzzy theory, physical programming, autonomous ground vehicle, human–machine mixed traffic.**

I. Introduction

AUTONOMOUS ground vehicles (AGVs) have a wide range of applications in military, industrial, and civilian domains and have become a key technology for developing safe and efficient transportation systems. According to the autonomous driving classification standard established by the Society of Automotive Engineers, autonomous driving technology is categorized into six levels, from Level 0 to Level 5 [1]. In recent years, leading companies are producing Level 5 Fully AGVs (FAGVs) without steering wheels and pedals to meet the demands of shared mobility, freight transportation, and public transit. In the coming years, it is only a matter of time before one of them launches the first commercially available AGV [2]. Additionally, [3] proposed a synergistic integrated FAGV-smart city holistic framework to truly make self-driving technology a harmonious part of our cities with sustainable urban development, and mentioned that "The developers of the FAGVs technology are claiming the safest driving on roads with the most experienced (self-) driver and promising a variety of benefits". This implies that with the development of AGV-related technologies, AGVs will gradually adapt to various traffic environments. In particular, their interaction capabilities with human-driven vehicles (HDVs) and other AGVs will steadily improve. As a result, the penetration rate of AGVs in mixed traffic is expected to increase gradually, and they are likely to drive the intelligent transformation of future transportation systems. Before the penetration rate of AGVs reaches 100%, HDVs and AGVs will coexist on the roads. This scenario can be referred to as a human-machine mixed traffic (HMMT) system. The coexistence of AGVs and HDVs in HMMT systems introduces new safety challenges, making the planning of safe and feasible trajectories a critical aspect of AGV autonomy design.

Among various trajectory planning tasks, lane-change serves as the foundation for driving maneuvers such as overtaking and U-turns, making it a significant research topic in HMMT systems. In HMMT environments, AGV lane-change trajectory planning must balance safety, feasibility, and computational efficiency, which has become a key research focus in this field.

In HMMT systems, understanding the intentions of HDV drivers (e.g., acceleration, deceleration) is crucial for planning safe and accurate trajectories for AGVs. This understanding facilitates the prediction of HDV motion trajectories, thereby enhancing the safety of AGV trajectory planning and reducing collision risks. To achieve this, as summarized in [4], methods such as support vector machine (SVM) and hidden Markov model (HMM) can be employed to quickly and accurately infer human driving intentions. However, the approach of first inferring driving intentions and then incorporating the

Received 20 December 2024; revised 21 April 2025; accepted 25 May 2025. Date of publication 23 June 2025; date of current version 21 October 2025. The Associate Editor for this article was Y. Wiseman. *(Corresponding author: Senchun Chai.)*

Gaochang Zhang, Zhida Xing, Runjiao Bao, Kun Liu, Yuanqing Xia, and Senchun Chai are with the School of Automation, Beijing Institute of Technology, Beijing 100081, China (e-mail: 3120215483@bit.edu.cn; xzd3120230854@bit.edu.cn; 3120230765@bit.edu.cn; kunliubit@bit.edu.cn; xia_yuanqing@bit.edu.cn; chaisc97@bit.edu.cn).

Yue Qiu is with Beijing Dongchezu Technology Company Ltd., Beijing 100007, China (e-mail: qiuyue.01@dcarlife.com).

Digital Object Identifier 10.1109/TITS.2025.3579233

predicted HDV trajectory into the planning process reduces the real-time performance of AGV trajectory generation.

Currently, AGV trajectory planning methods have been extensively studied, primarily including curve-based [5], [6], sampling-based [7], [8], [9], search-based [10], [11], and optimization-based [12], [13], [14] approaches. Among these, optimization-based methods have gained significant attention due to their superior ability to handle vehicle dynamic constraints and complex environmental limitations. However, optimization-based methods exhibit low computational efficiency in trajectory planning with obstacle avoidance constraints, making it challenging to meet real-time motion requirements. Moreover, in engineering practice, optimizing a single objective alone often fails to meet the requirements of decision-makers (DMs).

To address the above issues, this study proposes a self-attention guided convolutional neural network-long short-term memory network (CNN-LSTM) based multi-objective real-time trajectory planning framework for AGV lane-change in HMMT. In the framework, a multi-objective trajectory planning architecture that integrates interval type-2 fuzzy physical programming (IT2FPP) and a fitting function-based obstacle avoidance (FFOA) method is proposed to generate a dataset containing multi-objective optimal control actions for the AGV and the corresponding HMMT states under different HDV driving intentions. Then, a self-attention guided CNN-LSTM is proposed to learn the mapping relationship between the HMMT system states and AGV control actions, enabling multi-objective real-time trajectory planning with very low computational burden. Furthermore, since the intentions of HDV drivers are thoroughly considered during the creation of the dataset, there is no need to infer them when using this mapping relationship to generate AGV trajectory in real-time, further enhancing real-time performance. The contributions of this study can be summarized as follows:

1) The proposed FFOA method models obstacles using fitting functions, which has low complexity and improves computational efficiency while ensuring the generation of safe trajectories.
2) IT2PP treats all boundaries of the physical programming (PP) preference function as interval type-2 fuzzy numbers, effectively handling the uncertainties of these boundaries and the fuzzy preferences of multiple DMs.
3) The proposed self-attention guided CNN-LSTM network is specifically designed for time series data. This network effectively captures the features of time series data, ensuring high real-time performance in trajectory planning while enhancing the accuracy.
4) The framework proposed in this study fully incorporates HDV driving intentions during the dataset construction process, eliminating the need to inter them in real-time trajectory planning, further enhancing its real-time performance.

The remainder of this study is organized as follows: Section II reviews existing works related to this study. Section III introduces the FFOA method for constructing obstacle avoidance constraints and further develops a multi-objective trajectory planning model for AGV lane-change maneuvers in HMMT. Section IV presents the proposed IT2FPP method and self-attention guided CNN-LSTM, followed by an explanation of the real-time trajectory planning process using the proposed network. Section V conducts a series of simulations and physical experiments to demonstrate the effectiveness of our framework. Section VI further compares the proposed method with existing studies, highlighting its novelty, and discusses its limitations and potential improvements. The conclusions are summarized in Section VII.

To facilitate the reference of acronym definitions and better present the content of this study, we have included a list of acronyms, as shown in Tab. I.

TABLE I
LIST OF ACRONYMS

Acronym	Definition
AGV	autonomous ground vehicle
FAGV	Fully AGV
HDV	human-driven vehicle
HMMT	human-machine mixed traffic
SVM	support vector machine
HMM	hidden Markov model
DM	decision-maker
CNN	convolutional neural network
LSTM	long short-term memory
IT2FPP	interval type-2 fuzzy physical programming
FFOA	fitting function-based obstacle avoidance
PP	physical programming
MOTP	multi-objective trajectory planning
FPP	fuzzy physical programming
IT2FNs	interval type-2 fuzzy numbers
DNN	deep neural network
RDNN	recurrent deep neural network
GRU	gated recurrent unit
MSE	mean square error
FGP	fuzzy goal programming
WS	weighted sum
RMSE	root mean square error
HITL	human-in-the-loop
HOTL	human-on-the-loop

II. RELATED WORK

A. Human-Driven Vehicle Driving Intention Inference

To plan a safe and feasible trajectory for AGV in the HMMT, the key operation involves first inferring the HDV driving intentions and then integrating these intentions into AGV trajectory planning. With regard to the inference of human intentions, Chen et al. [15] employed a multi-SVM-based Dempster-Shafer framework to comprehend human gesture intentions. Gao et al. [16] developed a hybrid recurrent neural network architecture for human intention recognition. Yu et al. [17] proposed an LSTM-based neural network and experimentally validated its effectiveness in inferring human intentions. Moreover, Lu et al. [18] investigated human driving control behaviors using an HMM-based approach. Additionally, methods such as fuzzy control theory [19], Bayesian inference [20], and Gaussian mixture models [21] have also been explored for human intention recognition. Although these methods have been validated for their ability to accurately and quickly infer human intentions, the logic of "first inferring the HDV driving intentions and then integrating these intentions into AGV trajectory planning" inevitably adds time overhead.

This can result in a lag in AGV response in complex traffic scenarios, reducing the real-time performance of trajectory planning and even increasing the collision risk in emergency situations. To address this issue, we preemptively generate a dataset containing multi-objective optimal control actions for the AGV and the corresponding HMMT states under different HDV driving intentions. The proposed network is then employed to learn the mapping function between the HMMT system states and AGV control actions. Consequently, when using this mapping function for AGV trajectory planning, there is no need to infer HDV driving intentions, enabling faster real-time trajectory planning for the AGV.

B. Obstacle Avoidance Constraints

To avoid obstacles on the road, various obstacle avoidance constraint methods have been proposed. Chai et al. [22] applied an obstacle avoidance strategy based on the triangular area method and integrated it into a unified optimization framework. While this approach provides AGVs with great maneuverability and facilitates the search for an optimal solution, it suffers from low computational efficiency. Xing et al. [23] adopted a minimum bounding circle to approximate obstacles and construct avoidance constraints. They suggested using multiple circles to cover and approximate obstacles of different shapes to reduce conservativeness. However, when a large number of circular obstacles are set, the additional constraints increase the computational burden, leading to longer optimization times. Therefore, we propose a FFOA method to model the road and the HDVs considered as obstacles through fitting functions. This approach reduces the complexity of the obstacle avoidance constraints, thereby enhancing the efficiency of AGV trajectory pre-planning.

C. Multi-Objective Trajectory Planning

In AGV trajectory planning, optimization-based methods have gained widespread attention in recent years due to their effectiveness in handling various physical constraints and optimization objectives. Based on the number of optimization objectives, existing optimization-based trajectory planning methods can be classified into single-objective optimization and multi-objective optimization. Single-objective optimization methods focus on optimizing a single performance metric to generate feasible trajectories. Reference [24] selected the length of the determined trajectory as the minimization objective in the planning process, while Li et al. [25] and Chai et al. [26] minimized the completion time in order to achieve a safe and efficient trajectory for the AGV.

However, in practical trajectory planning for AGVs, considering only a single objective often fails to meet decision-making requirements, making multi-objective trajectory planning (MOTP) a research focus. To address MOTP problems, fuzzy physical programming (FPP), which integrates PP and fuzzy theory, is a useful tool. Unlike other multi-objective programming methods [27], [28] based on function transformation technique, PP-based methods do not require DMs to specify the weights of different objective functions or add additional constraints to express their preferences. References [29] and [30] treated one boundary of the PP preference function as a type-1 fuzzy number and constructed the fuzzy preference function through integration. However, this method can only handle uncertainty in one boundary and cannot express fuzzy preferences from multiple DMs. Qi et al. [31] constructed fuzzy preference functions by establishing a fuzzy value interval for the PP preference function and transforming boundaries into membership boundaries using membership functions. Similarly, this approach also cannot handle cases where all boundaries have uncertainty or express fuzzy preferences from multiple DMs. In contrast, this study proposes IT2FPP, where all boundaries of the PP preference function are considered as interval type-2 fuzzy numbers (IT2FNs). This approach effectively addresses situations where all boundaries of the PP preference function exhibit uncertainty and allows for the representation of fuzzy preferences from multiple DMs.

D. Neural Network Based Real-Time Trajectory Planning

Optimization-based methods are computationally intensive, limiting their real-time applicability. As a result, researchers have begun exploring neural network-based trajectory planning methods. The core idea is to first use optimization methods to generate an optimal trajectory dataset for specific task scenarios and then train a mapping function between vehicle states and optimal control actions. Once trained, the mapping function can be used for real-time AGV trajectory planning, improving planning efficiency. Mohammadpour et al. [32] considered the dynamic model of autonomous forklifts and employed a deep neural network (DNN) to predict optimal acceleration online, which was then integrated into a motion planning algorithm to generate energy-efficient and dynamically feasible trajectories. In [33], recurrent deep neural networks (RDNNs) were employed to approximate the mapping between vehicle states and optimal control actions, thereby developing a real-time motion planner for automatic parking tasks of AGVs. Reference [34] used LSTM-RDNN to implement real-time trajectory planning and control of AGVs. Huang et al. [35] proposed a real-time trajectory planner for logistical supply transportation using gated recurrent unit (GRU) neural networks. Xing et al. [23] proposed an online trajectory planner for AGVs based on LSTM-Attention network to handle sudden moving obstacles. The aforementioned studies have demonstrated the feasibility and real-time performance of neural network-based trajectory planning. However, these methods still face challenges in effectively extracting features from time series data in the optimal trajectory dataset and accurately fitting the mapping between vehicle states and optimal control actions. To address these challenges, a self-attention guided CNN-LSTM hierarchical network is proposed in this study, where the one-dimensional CNN is utilized for feature extraction and expansion, LSTM is employed to capture temporal dependencies, and the attention mechanism is applied to assign time-step weights to enhance feature representation. By leveraging these components, the proposed network effectively captures the features of time series data, ensuring high real-time performance in trajectory planning while enhancing the accuracy.

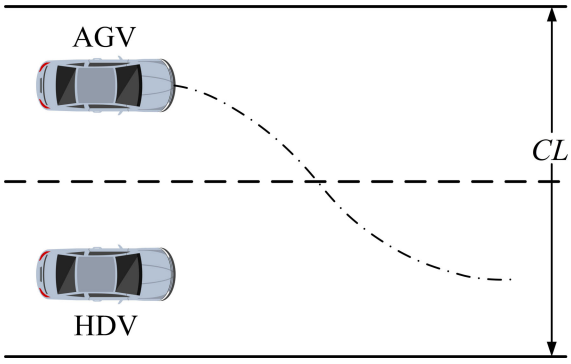

Fig. 1. The lane-change scenario of HMMT.

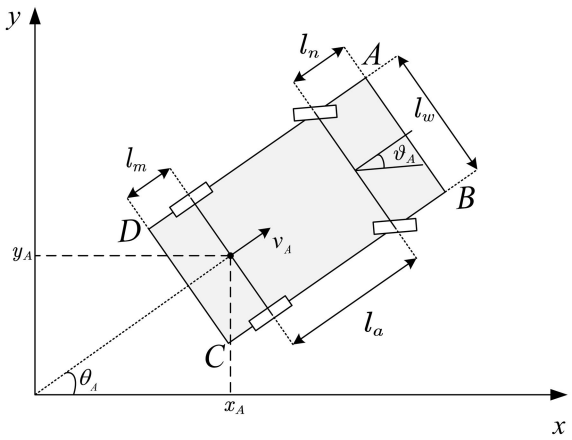

Fig. 2. Diagram of AGV body geometry and parameters.

III. Multi-Objective Trajectory Planning Problem Formulation of the Lane-Change Process

A. Human-Machine Mixed Lane-Change Traffic Motion Model

The general lane-change scenario of HMMT is visualized in Fig. 1, where CL represents the road width. Assuming that the HDV moves in a straight line and the well-known bicycle model [36] (as shown in Fig. 2) is used to describe the AGV's motion while neglecting effects such as sideslip caused by tire lateral forces, the overall motion of the HMMT system can be described by the following differential equations:

$$\begin{cases} \dot{x_A}(t) = v_A(t)\cos(\theta_A(t)), & \dot{y_A}(t) = v_A(t)\sin(\theta_A(t)) \\ \dot{\theta_A}(t) = v_A(t)\tan(\vartheta_A(t))/l_a, & \dot{v_A}(t) = a_A(t) \\ \dot{\vartheta_A}(t) = \omega_A(t), & \dot{x_H}(t) = v_H(t),\ \dot{v_H}(t) = a_H(t) \end{cases} \tag{1}$$

where (x_A, y_A) denotes the center point of the rear axle of the AGV; t represents time; v_A and a_A are the velocity and acceleration of the AGV; θ_A is the orientation of the AGV; ϑ_A represents the steering angle of the AGV, and ω_A is its angular velocity; l_a represents the distance between the front and rear wheels of the AGV; x_H, v_H and a_H represent the x-axis position, velocity, and acceleration of the HDV, respectively. In addition, a_H can be regarded as a concrete representation of the HDV driving intention.

The state variables of the HMMT system are defined as $X = [x_A, y_A, \theta_A, v_A, \vartheta_A, x_H, v_H]$ and the control inputs are defined as $U = [\boldsymbol{u}_A, \boldsymbol{u}_H] = [a_A, \omega_A, a_H]$. The remaining parameters of the vehicle are shown in Fig. 2, where l_n represents the length of the front overhang, l_m denotes the rear overhang length, and l_w is the vehicle width. A, B, C, D are the four vertices of the AGV. Since the vehicle is a rigid body, the coordinates (A_x, A_y), (B_x, B_y), (C_x, C_y), (D_x, D_y) of the four vertices can be calculated from (x_A, y_A), $\theta_A, l_n, l_m, l_a, l_w$:

$$\begin{cases} A_x(t) = x_A(t) + (l_a + l_n)\cos(\theta_A(t)) - 0.5l_w\sin(\theta_A(t)) \\ A_y(t) = y_A(t) + (l_a + l_n)\sin(\theta_A(t)) + 0.5l_w\cos(\theta_A(t)) \\ B_x(t) = x_A(t) + (l_a + l_n)\cos(\theta_A(t)) + 0.5l_w\sin(\theta_A(t)) \\ B_y(t) = y_A(t) + (l_a + l_n)\sin(\theta_A(t)) - 0.5l_w\cos(\theta_A(t)) \\ C_x(t) = x_A(t) - l_m\cos(\theta_A(t)) + 0.5l_w\sin(\theta_A(t)) \\ C_y(t) = y_A(t) - l_m\sin(\theta_A(t)) - 0.5l_w\cos(\theta_A(t)) \\ D_x(t) = x_A(t) - l_m\cos(\theta_A(t)) - 0.5l_w\sin(\theta_A(t)) \\ D_y(t) = y_A(t) - l_m\sin(\theta_A(t)) + 0.5l_w\cos(\theta_A(t)) \end{cases} \tag{2}$$

B. Various Types of Constraints

1) State/Control Constraints: Throughout the entire lane-change process, the states and control inputs of both the AGV and the HDV should be constrained and are represented as follows:

$$\begin{cases} x_{\min} \le x_A(t) \le x_{\max} & y_{\min} \le y_A(t) \le y_{\max} \\ \theta_{\min} \le \theta_A(t) \le \theta_{\max} & v_{\min} \le v_A(t) \le v_{\max} \\ \vartheta_{\min} \le \vartheta_A(t) \le \vartheta_{\max} & x_{\min} \le x_H(t) \le x_{\max} \\ v_{\min} \le v_H(t) \le v_{\max} & a_{\min} \le a_A(t) \le a_{\max} \\ c_{\min} \le c_A(t) \le c_{\max} & a_{\min} \le a_H(t) \le a_{\max} \end{cases} \tag{3}$$

where $c_A = \omega_A/(l_a\cos^2(\vartheta_A))$ represents the derivative of the instantaneous curvature of the AGV.

The aforementioned constraints ensure the safety and feasibility of AGV and HDV during the lane-change process. Since vehicles must remain within the lane boundaries and a certain length range during lane-change process, the lateral and longitudinal positions of AGV and the longitudinal position of HDV are constrained. Additionally, to prevent abnormal yawing or improper orientations within the lane, the heading angle θ_A of the AGV must be maintained within a reasonable range.

Moreover, considering vehicle dynamics, mechanical structure, and road traffic safety requirements, the velocities (v_A, v_H) and accelerations (a_A, a_H) of AGV and HDV must be appropriately constrained to prevent excessively high speeds or abrupt changes that could negatively impact vehicle stability and ride comfort. Furthermore, to ensure steering stability during the lane-change process, the rate of curvature variation must also be limited to prevent excessive changes that could lead to vehicle instability and compromise trajectory feasibility.

2) Obstacle Avoidance Constraints: To prevent the AGV from colliding with the road edges or the HDV during the lane-change process, this study proposes the FFOA method to

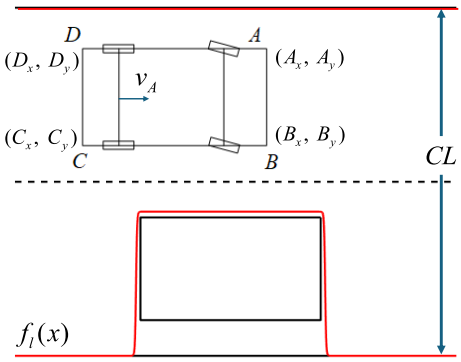

Fig. 3. Visualization of the FFOA method.

formulate obstacle avoidance constraints. As shown in Fig. 3, to ensure safety, the four vertices of the AGV must always remain within the two red boundary lines throughout the lane-change process. This can be expressed as:

$$\begin{cases} f_l(A_x(t)) \le A_y(t) \le CL \\ f_l(B_x(t)) \le B_y(t) \le CL \\ f_l(C_x(t)) \le C_y(t) \le CL \\ f_l(D_x(t)) \le D_y(t) \le CL \end{cases} \tag{4}$$

where CL is the road width, which defines the upper boundary of the AGV's feasible driving region, while $f_l(x)$ denotes the lower boundary. To fit the lower boundary, this study constructs the following fitting function based on the logarithmic Sigmoid function:

$$\begin{aligned} f_l(x) = & \left(\frac{a(x - x_H + l_1)}{2ln(e^{-a(x-x_H+l_1)} + e^{a(x-x_H+l_1)})} \right. \\ & \left. - \frac{a(x - x_H - l_2)}{2ln(e^{-a(x-x_H-l_2)} + e^{a(x-x_H-l_2)})} \right) \\ & * (y_H + 0.5l_w + \varepsilon) \end{aligned} \tag{5}$$

where $l_1 = l_m + \varepsilon$, $l_2 = l_a + l_n + \varepsilon$ and $y_H = CL/4$ represents the trajectory of the HDV moving along the x-axis.

In the fitting function, the parameters a and ε are used to adjust the steepness of the transition and the overall height of the curve, respectively. Specifically, a controls the steepness of the curve—larger values of a result in a sharper transition, approaching a step-like change, whereas smaller values lead to a smoother transition. The parameter ε influences the vertical offset of the curve. When $\varepsilon > 0$, the entire curve shifts upward, effectively adding an extra safety margin around the HDV. This encourages the AGV to adopt a more conservative obstacle avoidance strategy during trajectory planning, thereby reducing the risk of collisions. In this study, the two parameters are set to $a = 30$ and $\varepsilon = 0.1$.

3) Terminal Constraints: To ensure that the AGV maintains a safe distance and moves in a straight line with the HDV after changing lane, the following terminal constraints should be satisfied:

$$\begin{cases} \theta_A(t_f) = 0 & \text{(6a)} \\ y_A(t_f) = y_H & \text{(6b)} \\ d_{safe} \le |x_A(t_f) - x_H(t_f)| & \text{(6c)} \\ 0 \le |v_A(t_f) - v_H(t_f)| & \text{(6d)} \end{cases}$$

where d_{safe} represents the safe distance between the two vehicles and t_f is the terminal time. (6a) and (6b) ensure that after the AGV changes lane, it aligns with the HDV on a straight line. (6c) and (6d) ensure that after the AGV changes lane, it maintains a relatively safe distance and speed relative to the HDV. After the AGV changes lane and positions itself in front of the HDV, (6c) should be $d_{safe} \le x_A(t_f) - x_H(t_f)$ and (6d) should be $0 \le v_A(t_f) - v_H(t_f)$; On the contrary, (6c) should be $d_{safe} \le x_H(t_f) - x_A(t_f)$ and (6d) should be $0 \le v_H(t_f) - v_A(t_f)$.

C. Multi-Objective Trajectory Planning Problem

In practical lane-change trajectory planning scenarios, optimizing a single performance metric alone is insufficient to meet the needs of DMs. Therefore, this study considers the simultaneous optimization of multiple performance metrics. Building upon the previous discussion, the formulation of the multi-objective trajectory planning problem is presented as follows:

$$\begin{aligned} \min \ & \mathbb{F} = [F_1(t), F_2(t), \dots F_n(t)] \\ \text{s.t.} \ & \text{Eq. (1) - Kinematic constraints} \\ & \text{Eq. (3) - State/control constraints} \\ & \text{Eq. (4) - Obstacle avoidance constraints} \\ & \text{Eq. (6) - Terminal constraints} \end{aligned} \tag{7}$$

where $\mathbb{F} \in \mathbb{R}^n$ is the objective function vector, and n is the number of objective functions. (7) represents the general form of continuous-time multi-objective trajectory planning problem. After discretization, multi-objective optimization methods can be applied to integrate multiple objectives, followed by solving with a numerical optimization solver.

D. Optimization Objectives

In this study, we aim to minimize the time required for the AGV to complete the lane-change task while maximizing passenger comfort. Therefore, the optimization objectives are defined as follows:

(1) Minimize the completion time:

$$\min \ F_1(t) = t_f \tag{8}$$

(2) Maximize passenger comfort [37]:

$$\min \ F_2(t) = \int_{t=0}^{t_f} \left(a_A^2(t) + v_A^2(t)\omega_A^2(t) \right) dt \tag{9}$$

A smaller value of F_1 corresponds to a shorter time for the vehicle to change lane. F_2 is derived from the ISO 2631-1 standard, which evaluates automobile comfort. By minimizing acceleration, linear velocity, and angular velocity along the trajectory, this leads to a smoother trajectory. Consequently, a smaller F_2 results in greater passenger comfort.

E. Problem Discretization

To train the mapping function between the HMMT system states and the control actions of the AGV, we need a finite amount of data to construct the relevant dataset. In this

study, we use the pseudospectral collocation method [38], often applied in AGV control, to convert the continuous-time HMMT trajectory planning problem into a nonlinear static problem. This method involves discretizing system states and controls at specific temporal nodes $\{t_k\}_{k=1}^{k=N_k}$ with $X(t_k) = X_k$ and $U(t_k) = U_k$. Consequently, the optimization objectives, motion equations, and different constraints are expressed either as functions of the parameterized state and control or as values at these collocation nodes. This transformation simplifies the original optimal lane-change maneuver problem into a static constrained problem, solvable with standard optimization techniques. Specifically, the optimization task is to determine (X_k, U_k) at each temporal node t_k, $k = 1, \ldots, N_k$, to optimize the discretized performance indexes and satisfy the discretized constraints.

Remark 1: For the N_k temporal nodes, the method used in [22] requires $16N_k$ constraints to achieve obstacle avoidance in the scenario shown in Fig. 1. The method in [23], when using a circle to represent the HDV, also requires $16N_k$ constraints. In contrast, as shown in (4), the FFOA method employed in this study only requires $8N_k$ constraints, reducing the complexity of the obstacle avoidance constraints and improving computational efficiency.

IV. Multi-Objective Real-Time Trajectory Planning Framework

A. Interval Type-2 Fuzzy Physical Programming

In order to solve the discretized multi-objective optimization problem (7), PP is a useful tool. The crucial elements of PP are preference functions, which are employed to capture the preferences of DM. Generally, preference functions in PP are divided into the following four types: (1) Smaller is better; (2) Larger is better; (3) Closer to a value is better; (4) Closer to a range is better.

In contrast to other multi-objective programming methods based on function transformation techniques, PP does not require DMs to specify the weights of different objective functions or add additional constraints to express their preferences. Instead, taking the "smaller is better" type of preference function as an example, the DM needs to utilize five boundary values to divide preferences into six continuous intervals representing different levels of satisfaction, namely the Ideal Level, Desirable Level, Tolerable Level, Undesirable Level, Highly undesirable Level, and Unacceptable Level, which is shown in Fig. 4. Once the five boundaries $F_{i,1}$, $F_{i,2}$, $F_{i,3}$, $F_{i,4}$, $F_{i,5}$ of the i-th objective function are designed by the DM, the continuous increasing preference function $G(F_i)$ can be constructed using a quartic polynomial fitting method. The construction process can refer to [39]. This function represents a mapping from the F_i -axis to the G_i-axis shown as the curve in Fig. 4.

In order to incorporate multiple DMs' intuitive grasp of the desired design outcomes and handle the cases where all boundaries of the PP preference functions exhibit uncertainty, this study extends FPP to IT2FPP, which considers all boundaries of the PP preference function as trapezoidal IT2FNs denoted as $\tilde{F}_{i,1}$, $\tilde{F}_{i,2}$, $\tilde{F}_{i,3}$, $\tilde{F}_{i,4}$, $\tilde{F}_{i,5}$. As shown in Fig. 4, a trapezoidal

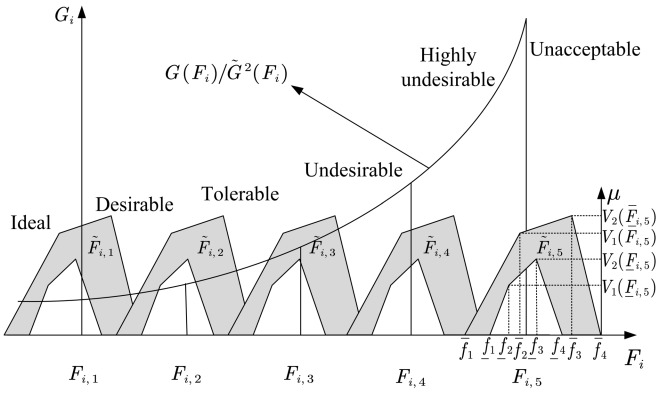

Fig. 4. PP/IT2FPP preference function.

IT2FN $\tilde{F}_{i,5}$ can be defined as

$$\tilde{F}_{i,5} = [\bar{F}_{i,5}, \underline{F}_{i,5}] = [\bar{f}_1, \bar{f}_2, \bar{f}_3, \bar{f}_4; V_1(\bar{F}_{i,5}), V_2(\bar{F}_{i,5}), \underline{f}_1, \underline{f}_2, \underline{f}_3, \underline{f}_4; V_1(\underline{F}_{i,5}), V_2(\underline{F}_{i,5})] \tag{10}$$

where $\bar{F}_{i,5}$, $\underline{F}_{i,5}$ represent the upper and lower type-1 fuzzy numbers, respectively. $V_m(\bar{F}_{i,5})$ and $V_m(\underline{F}_{i,5})$ refer to the membership values of the respective elements $\bar{f}_{m+1}$ and $\underline{f}_{m+1}$ with $m = 1, 2$. According to [40], the expected value $\bar{F}_{i,5}$ of the IT2FN $\tilde{F}_{i,5}$ is calculated as follow:

$$\bar{F}_{i,5} = H(\tilde{F}_{i,5}) = \frac{1}{2}\left(\frac{1}{4}\sum_{m=1}^{4}\left(\underline{f}_m + \bar{f}_m\right)\right) \times \frac{1}{4}\left(\sum_{m=1}^{2}\left(V_m(\underline{F}_{i,5}) + V_m(\bar{F}_{i,5})\right)\right) \tag{11}$$

$\bar{F}_{i,1}$,$\bar{F}_{i,2}$, $\bar{F}_{i,3}$, $\bar{F}_{i,4}$ can be obtained in the same way. Next, we replace the five original boundaries $F_{i,1}$, $F_{i,2}$, $F_{i,3}$,$F_{i,4}$,$F_{i,5}$ with $\bar{F}_{i,1}$,$\bar{F}_{i,2}$, $\bar{F}_{i,3}$, $\bar{F}_{i,4}$, $\bar{F}_{i,5}$ to construct the interval type-2 fuzzy preference function, denoted as $\tilde{G}^2(\bar{F}_i)$.

Then, following the approach of integrating objective functions in PP in [39], the IT2FPP model for the multi-objective trajectory planning problem considered in this study is formulated as follows:

$$\begin{aligned} &\min \ \log_{10}\left\{\frac{1}{n}\sum_{i=1}^{n}\tilde{G}^2(\bar{F}_i)\right\} \\ &\text{s.t. All aforementioned constraints} \\ &\quad \text{in their discretized form} \end{aligned} \tag{12}$$

At this point, (12) can be solved using traditional numerical optimization methods to obtain the corresponding pre-planning trajectories.

B. Establishment of Dataset

Before constructing the network model, a dataset $\mathbb{T}$ comprising N_t optimized histories of the AGV control evolution and the HMMT state histories is pre-generated. This can be achieved by uniformly sampling HDV driving intentions manifested through vehicle accelerations and planning corresponding optimal trajectories. That is, the IT2FPP problem (12) is iteratively solved with $a_H = a_{\min} : \beta : a_{\max}$,

Algorithm 1 Dataset $\mathbb{T}$ Generation

Input: Dataset size N_t, sampling interval β, optimization tolerance ϵ
procedure
  Initialize $\mathbb{T} = \emptyset$
  for $a_H = a_{\min} : \beta : a_{\max}$ **do**
    Address the IT2FPP problem (12) via numerical optimization solver.
    if optimization tolerance ϵ is satisfied **then**
      $\mathbb{T} = \mathbb{T} \cup \{X_k^*, \boldsymbol{u}_{A,k}^* = (a_{A,k}^*, \omega_{A,k}^*)\}$
    else
      $\mathbb{T} = \mathbb{T} \cup \emptyset$
    end if
  end for
end procedure
Output: $\mathbb{T}$

where $\beta = (a_{\max} - a_{min})/(N_t - 1)$ is sampling interval and is determined by DMs. Note that, this study assumes human intentions remain unchanged once manifested and the initial $a_H = 0$. Furthermore, a threshold γ is set for a_H. When $a_H \leq \gamma$, the AGV is positioned ahead of the HDV after completing the lane-change, whereas when $a_H > \gamma$, the AGV is positioned behind the HDV. The process of constructing the dataset $\mathbb{T}$ is detailed in Algorithm 1.

Remark 2: The computational complexity of Algorithm 1 depends on the dataset size N_t and the numerical optimization method used to solve the IT2FPP problem. In this study, we employ the Sequential Quadratic Programming (SQP) method to obtain the optimal lane-change trajectory. Given that the SQP algorithm runs for K iterations, with N_v decision variables and N_c constraints, the computational complexity of a single iteration can be approximated as $(N_v + N_c)^3$. Consequently, the overall computational complexity of Algorithm 1 is $\mathcal{O}(N_t \cdot K \cdot (N_v + N_c)^3)$. To enhance efficiency in dataset construction, we incorporate a warm-start strategy when solving the optimization problem using SQP, providing a reasonable initial guess to accelerate convergence. This approach significantly reduces the number of SQP iterations K, lowering computational costs while ensuring optimization stability, thereby improving dataset construction efficiency. Furthermore, to further optimize computational performance, parallel computing strategies can be employed during dataset construction, enabling efficient execution of optimization processes in a multi-threaded environment.

Remark 3: : The entire dataset $\mathbb{T}$ consists of N_t optimal lane-change trajectories covering various scenarios. Each trajectory comprises the state variables X_k of the HMMT system and the control variables $\boldsymbol{u}_{A,k} = (a_{A,k}, \omega_{A,k})$ of the AGV. This dataset $\mathbb{T}$ is used to train the designed network, where the system state X_k serves as the input and the AGV control variables $\boldsymbol{u}_{A,k}$ as the output. The physical significance of this approach lies in enabling the trained network to generate AGV lane-change control commands directly based on the observed state of the HMMT system. This allows the AGV to execute autonomous lane-change without the need to infer the human driver's intention within the HDV before making decisions.

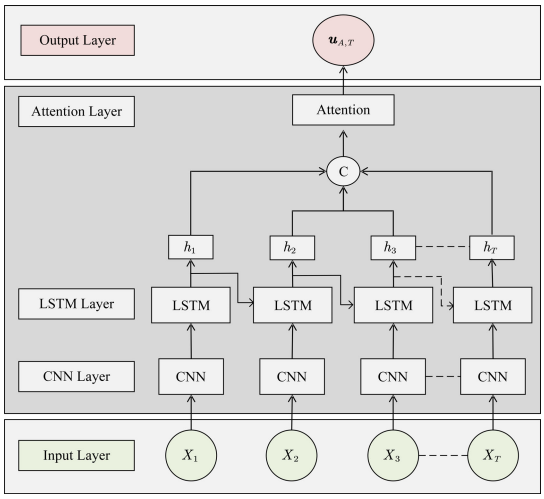

Fig. 5. Network architecture.

C. Self-Attention Guided CNN-LSTM Network Structure

To process complex time series data in the HMMT system, the network architecture presented in this study (shown in Fig. 5) is an integrated model that combines CNN, LSTM, and attention mechanism. This design effectively extracts features, captures temporal dependencies, and emphasizes key information points. Unlike existing CNN-LSTM-Attention networks [41], [42], the proposed network is specifically optimized for time series data, allowing for more effective extraction of intrinsic features from sequential state data and improving the accuracy of trajectory planning.

The CNN extracts features from the input time series data through the convolution layer. The convolution kernel (or filter) in the convolution layer slides on the data and extracts local features by calculating the dot product between the convolution kernel and the local area of the data. By stacking multiple convolution layers, higher-level features can be gradually extracted. These features are more abstract and complex than the original data, which is beneficial for subsequent processing tasks. In this study, one-dimensional CNN is employed to process the state time series data of the HMMT system. We regard different features in the time series data as different spatial positions in the spatial domain and exploit the ability of CNNs to capture local patterns and hierarchical structures to process time series features, which provides richer information for the subsequent LSTM network and attention mechanism.

LSTM greatly mitigates the vanishing gradient and exploding gradient problems that traditional recurrent neural networks are prone to during training by introducing three key gating mechanisms: the forget gate, the input gate, and the output gate.

In a typical LSTM network, the computation process of the three gating mechanisms at time step t_k is as follows:

$$f_k = \sigma(W_f \cdot [h_{k-1}, \mathcal{X}_k] + b_f)$$
$$i_k = \sigma(W_i \cdot [h_{k-1}, \mathcal{X}_k] + b_i)$$

$$
\begin{aligned}
o_k &= \sigma(W_o \cdot [h_{k-1}, \mathcal{X}_k] + b_o) \\
\tilde{C}_k &= \tanh(W_C \cdot [h_{k-1}, \mathcal{X}_k] + b_C) \\
C_k &= f_k * C_{k-1} + i_k * \tilde{C}_k \\
h_k &= o_k * \tanh(C_k)
\end{aligned} \tag{13}
$$

where $\mathcal{X}_k$ is the sequence data output from the CNN. f_k, i_k, and o_k represent the forget gate, input gate, and output gate, respectively. $\{W_f, W_i, W_o\}$ and $\{b_f, b_i, b_o\}$ denote the weights and biases of different gates. h_{k-1} and h_k represent the hidden states at the previous and current time steps, respectively, while $\tilde{C}_k$ and C_k denote the candidate state and cell state at time step t_k. $\sigma(\cdot)$ and $\tanh(\cdot)$ refer to the sigmoid activation function and the hyperbolic tangent activation function, respectively. These gating mechanisms enable the LSTM network to selectively learn, retain, and forget information, thereby effectively capturing long-term dependencies.

The attention mechanism allows the model to dynamically adjust the focus on outputs of different time steps when processing time series data. By assigning different weights (i.e., attention scores) to outputs of different time steps, the model can focus on the information that is most critical to the current task and ignore unimportant information. The introduction of the attention mechanism makes the model more efficient and accurate when processing complex time series data. By focusing on key information, the model can converge to the optimal solution faster and is more robust to noise and outliers.

In this study, a multi-head attention mechanism is employed to further extract features from the hidden state sequence output by the LSTM network, denoted as $H = [h_1, h_2, \ldots, h_T] \in \mathbb{R}^{T \times d_h}$. Given h_s attention heads, the computation process for the i-th attention head is as follows:

1) Compute the query $Q^{(i)}$, key $K^{(i)}$, and value $V^{(i)}$:

$$
Q^{(i)} = HW_Q^{(i)}, \quad K^{(i)} = HW_K^{(i)}, \quad V^{(i)} = HW_V^{(i)} \tag{14}
$$

where $W_Q^{(i)}, W_K^{(i)}, W_V^{(i)} \in \mathbb{R}^{d_h \times d_k}$ are linear transformation matrices, and d_k represents the dimension of the query, key, and value in the attention mechanism.

2) Compute the attention weights $A_W^{(i)}$:

$$
A_W^{(i)} = \text{softmax}\left(\frac{Q^{(i)}(K^{(i)})^{\mathrm{T}}}{\sqrt{d_k}}\right) \tag{15}
$$

3) Compute the attention output $O^{(i)}$:

$$
O^{(i)} = A_W^{(i)} V^{(i)} \tag{16}
$$

After computing the outputs of all attention heads, they are concatenated and transformed linearly to obtain the final attention output:

$$
O_a = [O^{(1)}, O^{(2)}, \ldots, O^{(h_s)}]W_O \tag{17}
$$

where W_O is the output mapping matrix.

D. Training of the Self-Attention Guided CNN-LSTM Network

After defining the proposed network architecture, data normalization is applied to enhance training stability and convergence. In this study, Min-Max normalization is used to scale the input data to the range [0, 1], mitigating the impact of varying magnitudes. The mathematical formulation of Min-Max normalization is as follows:

$$
X_k^{norm} = \frac{X_k - \min(X_k)}{\max(X_k) - \min(X_k)} \tag{18}
$$

where $\min(\cdot)$ and $\max(\cdot)$ denote the minimum and maximum operations, respectively.

To ensure that the parameters in the proposed network can be effectively updated through backpropagation and gradient descent, we follow most neural network-based trajectory planning studies and adopt the mean square error (MSE) as the loss function for network training. The MSE loss function is formulated as follows:

$$
MSE_{loss} = \frac{1}{N_t}\sum_{i=1}^{N_t}\left(\frac{1}{n_i}\sum_{j=1}^{n_i}(\boldsymbol{u}_{A,j} - \hat{\boldsymbol{u}}_{A,j})^2\right) \tag{19}
$$

where n_i represents the number of trajectory points in each trajectory, while $\boldsymbol{u}_{A,j}$ and $\hat{\boldsymbol{u}}_{A,j}$ denote the optimal control from the dataset and the output control of the network, respectively.

E. Real-Time Trajectory Planning

Using the proposed network, the mapping function $N_u(\cdot)$ could be trained to approximate the optimal control action $\boldsymbol{u}_{A,k}$ at t_k of the AGV with the HMMT system state X_k at t_k as the input, i.e.,

$$
\boldsymbol{u}_{A,k} :\approx N_u(X_k) \tag{20}
$$

Then, whenever the state X_k of the HMMT system at t_k is obtained, we can quickly plan the optimal control action $\boldsymbol{u}_{A,k}$ at t_k for the AGV using (20). Therefore, the mapping function $N_u(\cdot)$ can be used as a real-time trajectory planner for the AGV in the lane-change scenario of HMMT. Note that, since the dataset we have constructed includes human driver intentions, employing the mapping function $N_u(\cdot)$ for AGV trajectory planning eliminates the need to speculate on human driver intentions, further enhancing the planning efficiency. The algorithmic steps are summarized in Algorithm 2.

Remark 4: The computational complexity of Algorithm 2 depends on the number of trajectory points N_k as well as the network's hierarchical structure and parameter configuration. In the self-attention guided CNN-LSTM architecture, let the input time series data sequence length be L_q, the convolution kernel size of the one-dimensional CNN be K_C, the input vector dimension be N_{in}, and the output vector dimension be N_{out}. The computational complexity of the CNN component is then given by $\mathcal{O}(L_q \cdot K_C \cdot N_{in} \cdot N_{out})$. For the LSTM component, which further processes the features extracted by the CNN, let the hidden layer dimension be N_h. The computational complexity of the LSTM is $\mathcal{O}(L_q \cdot N_h^2)$. The self-attention mechanism operates on the hidden state sequence output by the LSTM, with a computational complexity of approximately $\mathcal{O}(L_q^2 \cdot N_h)$. Therefore, the overall computational complexity of Algorithm 2 can be expressed as:

$$
\mathcal{O}(N_k \cdot (L_q \cdot K_C \cdot N_{in} \cdot N_{out} + L_q \cdot N_h^2 + L_q^2 \cdot N_h))
$$

Algorithm 2 Real-Time Planning Process

Input: Number of trajectory points N_k, time points $\{t_k\}_{k=1}^{k=N_k}$
procedure
  for each time point $t_k, k = 1, 2, \ldots, N_k$ **do**
    Measure the actual state X_k of the HMMT system.
    Get the motion command $\boldsymbol{u}_{A,k}$ via

$$\boldsymbol{u}_{A,k} :\approx N_u(X_k)$$

    Apply $\boldsymbol{u}_{A,k}$ to the discretized equation (1).
    Record the trajectory point of AGV, update the time point $t_k \rightarrow t_{k+1}$, and go back to step 4.
  end for
end procedure
Output: Planned trajectory

TABLE II
SIMULATION PARAMETERS

Parameter	Value/Range	Parameter	Value/Range
d_{safe}	45 m	l_w	1.771 m
l_m	0.657 m	l_a	2.588 m
l_n	0.839 m	$[x_{\min}, x_{\max}]$	$[0, 500]$ m
$[y_{\min}, y_{\max}]$	$[0, 6]$ m	$[\theta_{\min}, \theta_{\max}]$	$[-90, 90]$ deg
$[v_{\min}, v_{\max}]$	$[5, 20]$ m/s	$[\vartheta_{\min}, \vartheta_{\max}]$	$[-33, 33]$ deg
$[a_{min}, a_{max}]$	$[-0.75, 0.75]$ m/s^2	$[c_{min}, c_{max}]$	$[-0.6, 0.6]$ rad/(m · s)

In neural network-based trajectory planning methods, the sequence length of time series data is generally small, leading to relatively low computational complexity and ensuring real-time feasibility for AGV lane-change maneuvers. Furthermore, subsequent experiments in this study confirm the proposed network's real-time performance and effectiveness in trajectory planning tasks.

V. SIMULATION AND PHYSICAL EXPERIMENT RESULTS

A. Simulation Settings

The simulation parameters employed in this study are summarized in Tab. II. The scenario is depicted in Fig. 1. The AGV and HDV have identical physical structures and start at positions (0 m, 4.5 m) and (0 m, 1.5 m), respectively. It is assumed that when $a_H \leq 0.2$ m/s^2, after the AGV changes lanes, it is positioned in front of the HDV; conversely, the AGV would position itself behind the HDV. In addition, $\beta = 0.0001$.

In constructing the interval type-2 preference functions for each objective function, this study uniformly partitions the value range of each objective function as the initial boundaries of the preference function, i.e.,

$$[F_{1,1}, F_{1,2}, F_{1,3}, F_{1,4}, F_{1,5}] = [0, 12.5, 25, 37.5, 50]$$
$$[F_{2,1}, F_{2,2}, F_{2,3}, F_{2,4}, F_{2,5}] = [0, 10, 20, 30, 40]$$

And these boundary values can be estimated as IT2FNs, i.e.

$$\tilde{F}_{1,1} = (-1.5, 0, 2, 3; 0.99, 1.00) \quad (-1, 0.5, 1.5, 2.5; 0.98, 0.97);$$
$$\tilde{F}_{1,2} = (10.5, 12, 14, 15; 0.96, 0.98) \quad (11.5, 12.5, 13.5, 14.5; 0.93, 0.92);$$
$$\tilde{F}_{1,3} = (23.1, 24.5, 26.5, 27.4; 0.98, 0.97) \quad (24, 25.3, 26, 27.1; 0.93, 0.96);$$
$$\tilde{F}_{1,4} = (35.7, 37.1, 39, 40.1; 0.95, 0.97) \quad (36.4, 37.5, 38.3, 39.5; 0.94, 0.93);$$
$$\tilde{F}_{1,5} = (47.8, 49.6, 50.5, 51.5; 0.96, 0.98) \quad (48.9, 49.1, 50, 51; 0.94, 0.93);$$
$$\tilde{F}_{2,1} = (-2, -0.5, 1.5, 2.5; 1.00, 0.99) \quad (-1, 0, 1.2, 2; 0.98, 0.98);$$
$$\tilde{F}_{2,2} = (8.1, 9.5, 11.3, 12.5; 0.98, 0.99) \quad (9, 10, 11.1, 12.2; 0.96, 0.95);$$
$$\tilde{F}_{2,3} = (18, 19.5, 21.5, 22.5; 0.98, 0.97) \quad (19, 20, 21, 22; 0.92, 0.93);$$
$$\tilde{F}_{2,4} = (28.1, 29.4, 31.6, 32.6; 0.95, 0.97) \quad (29, 30.1, 31.2, 32; 0.93, 0.91);$$
$$\tilde{F}_{2,5} = (38, 39.5, 41.5, 42.5; 0.96, 0.98) \quad (39, 40, 41, 42; 0.94, 0.92).$$

Remark 5: $[0, 50]$ are the minimum and maximum values set for F_1. Similarly, $[0, 40]$ are the minimum and maximum values set for F_2. All IT2FNs are determined based on the fuzzy preferences of multiple DMs. In this study, we define these IT2FNs based on the fuzzy preferences expressed by all the authors.

In this study, the offline training of all networks was conducted on an NVIDIA V100 GPU. Once the networks were trained for online trajectory planning, real-time inference and planning were performed on a personal computer with Windows 11, equipped with an Intel Core i7-9750H processor (2.60 GHz) and 16 GB of RAM.

B. Performance Analysis of Multi-Objective Trajectory Planning

To verify the effectiveness of the proposed IT2FPP method in MOTP for AGV lane-change scenarios, a comparative study is conducted between different multi-objective and single-objective trajectory planning methods under identical experimental conditions. Specifically, this study designed four different experimental scenarios, each with a distinct HDV acceleration configuration. The HDV acceleration values are randomly selected from the following four ranges: $[-0.3, 0]$ m/s^2 (shown as Fig. 6a), $[0, 0.2]$ m/s^2 (shown as Fig. 6b), $[0.2, 0.5]$ m/s^2 (shown as Fig. 6c), and $[0.5, 0.7]$ m/s^2 (shown as Fig. 6d). Each method is required to optimize either multi-objective or single-objective lane-change trajectories without collision risks under these four acceleration conditions to evaluate their adaptability and optimization performance. The MOTP methods, including IT2FPP, FPP1 [31], FPP2 [29], [30], fuzzy goal programming (FGP) [27], and weighted sum (WS) [28], are designed to simultaneously optimize travel time and passenger comfort, whereas the single-objective trajectory planning methods focus solely on minimizing travel time [25] or maximizing passenger comfort. As shown in Fig. 6, the trajectory curves under different scenarios are compared in detail, while Fig. 7 further quantifies

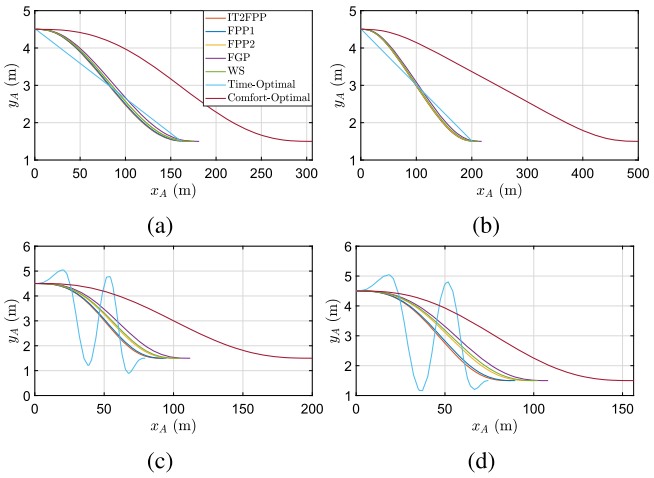

Fig. 6. Comparison of AGV trajectories under different optimization methods and objectives. (In experimental scenarios with HDV acceleration configurations within the range of $[0.2, 0.5]$ m/s^2 and $[0.5, 0.7]$ m/s^2, the trajectory optimized using the single-objective trajectory planning method that minimizes travel time requires maintaining the maximum speed as much as possible. However, to avoid collisions with the HDV, the AGV cannot immediately change lane, leading to the need for continuous steering adjustments. As a result, the planned trajectory exhibits a distinct curved shape.)

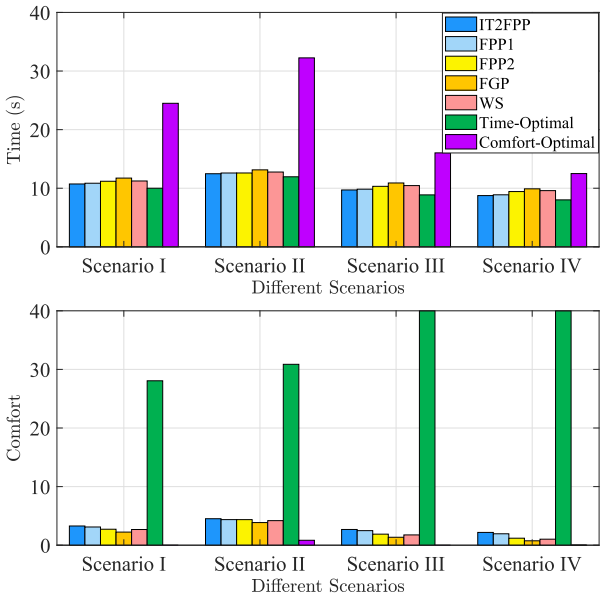

Fig. 7. Time and passenger comfort of trajectories planned by different methods in various scenarios. (In Scenario I, III, and IV, when comfort maximization is set as the sole optimization objective, the AGV adopts near-zero acceleration and steering angular velocity to achieve optimal comfort while satisfying all constraints. Due to the extremely smooth trajectory variations, the final comfort index value is extremely low, approaching zero.)

and illustrates the numerical differences in maneuver time and passenger comfort for trajectories generated by different optimization methods.

As illustrated in the Fig. 6 and Fig. 7, when the single-objective method prioritizes only travel time, the resulting trajectory lacks smoothness, leading to a significant decrease in passenger comfort. Conversely, when optimizing solely for passenger comfort, the time required to complete the lane-change task increases significantly, which is not conducive to quick and safe lane-change. In contrast, the trajectory designed by the MOTP methods effectively balances the two objectives of time and comfort. It ensures the smoothness of the trajectory while achieving a travel time only slightly longer than the shortest time obtained from single-objective optimization. However, WS cannot handle fuzzy factors, FGP cannot express the preferences of multiple DMs, and FPP1 and FPP2 cannot handle cases where all boundaries have uncertainty or express fuzzy preferences from multiple DMs. In comparison, the IT2FPP method has the advantage of being able to handle situations where all boundaries of the preference function exhibit uncertainty, while also accommodating fuzzy preferences from multiple DMs.

C. Implementation of a Real-Time Trajectory Planner Based on the Self-Attention Guided CNN-LSTM Network

To achieve optimal real-time trajectory planning performance, it is necessary to adjust the network's architecture and parameters. In this study, under the self-attention guided CNN-LSTM network framework, different network parameter combinations are tested. The optimality of the network's actual planned trajectories is used as the evaluation criterion for selection, resulting in the final designed network's hyperparameters, as shown in Tab. III.

TABLE III
NETWORK HYPERPARAMETERS

Hyperparameters	Value
Input channels for Conv1D layer	7
Kernel size of Conv1D layer	1
Output channels for Conv1D layer	64
Input dimension for LSTM layer	64
Hidden state dimension of LSTM layer	64
Input/Output dimension of Attention mechanism	64
Number of heads in Multi-Head Attention	8
Dropout probability	0.1

D. Comparison of Different Network-Based Real-Time Trajectory Planning Methods

The proposed self-attention guided CNN-LSTM network effectively combines CNN, LSTM, and attention mechanism, enabling deep feature extraction and temporal information capture while focusing on important features and temporal segments. This integration enhances the accuracy of the network's trajectory planning for the specified tasks. To validate the superiority and accuracy of the proposed network, it is compared with optimization-based method (Reference), CNN-LSTM-based method [43], LSTM-Attention-based method [23], LSTM-RDNN-based method [34], GRU-based method [35], RDNN-based method [33], and DNN-based method [32]. It is worth noting that in [43], CNN-LSTM was used for trajectory prediction. However, it shares some components with the network proposed in this study, except for the absence of attention mechanism. Therefore, a comparison is also made with this network. In the same task scenario, with the acceleration of the HDV set to 0.201 m/s^2, different methods are used to design lane-change trajectory planning for this problem.

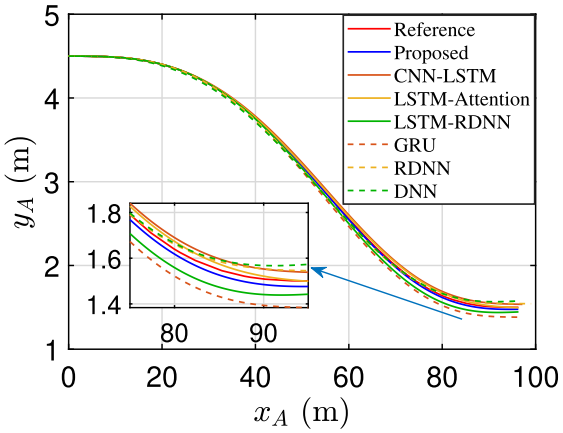

Fig. 8. Comparison of lane-change trajectories designed by different methods.

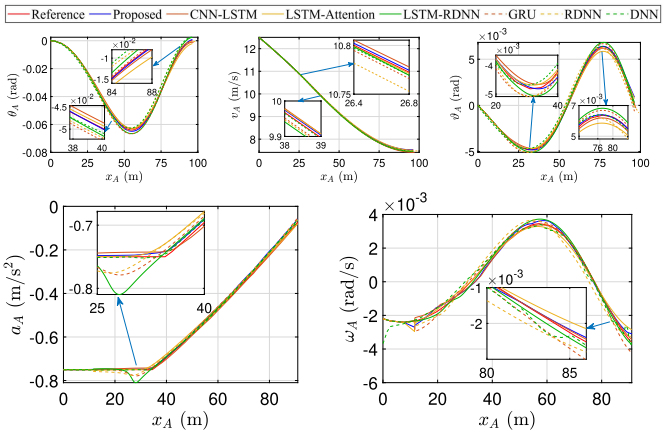

Fig. 9. State and control curves of trajectories designed by different methods.

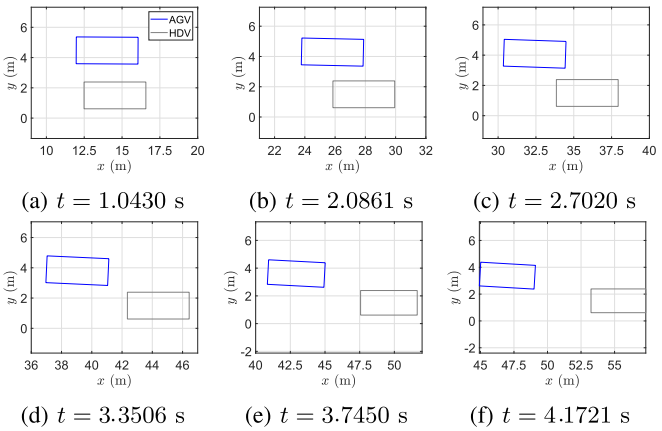

Fig. 10. Lane-change process diagram of the trajectory designed by the self-attention guided CNN-LSTM network.

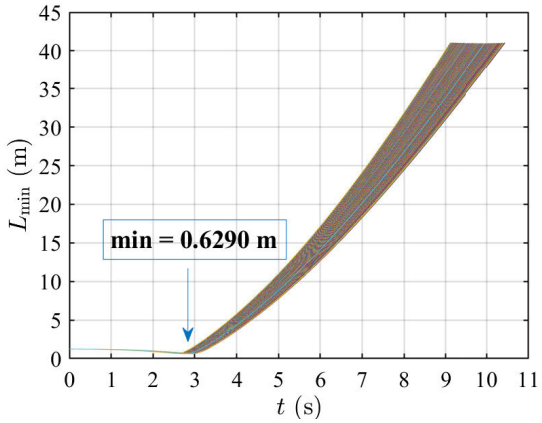

Fig. 11. The minimum distance between the AGV and HDV during the lane-change process.

Fig. 8 presents the comparison of lane-change trajectories designed by different methods. As shown in the figure, all methods can generate feasible lane-change trajectories, but the degree of alignment with the optimal trajectory varies, especially at the terminal position of the trajectories. The closer the network-based methods are to generating trajectories that closely align with the optimal trajectory, the more knowledge the network has learned about optimal lane-change trajectory design. As shown in Fig. 8, compared to other methods, the lane-change trajectory designed by the proposed method is closer to the optimal trajectory because it combines CNN, LSTM, and attention mechanism, specifically designed to deeply mine the features of sequential data. This enables more efficient feature extraction, resulting in a more accurate representation of the mapping relationship between the HMMT system states and the optimal control actions. Additionally, Fig. 9 illustrates the state and control curves of the lane-change trajectories designed by different methods. It can be observed that, except for the LSTM-RDNN, GRU, and RDNN-based methods, which show slight violations in acceleration constraints, all other methods satisfy the predefined constraints for all state and control variables.

To demonstrate the safety of the lane-change trajectory designed using the proposed method, Fig. 10 shows the relative positions of the AGV and HDV at several key moments during the lane-change process. The figure illustrates that, under the guidance of the proposed method, the AGV successfully completes the lane-change task, avoiding collisions with the HDV in the target lane.

Furthermore, to further evaluate the safety of the lane-change trajectories generated by the proposed algorithm, Fig. 11 presents the variation in the minimum distance between the AGV and the HDV throughout the motion process across 300 different lane-change tasks. The experimental results show that the AGV consistently maintains a safe distance from the HDV in all lane-change tasks, with the minimum distance between them never falling below 0.629 m throughout the entire test. These findings validate the safety and broad applicability of the proposed method in lane-change trajectory planning.

Neural network-based trajectory planning methods are trained based on an optimal trajectory dataset, with the goal of efficiently planning trajectories that match those designed using optimization methods in real-time. Therefore, to further quantitatively compare the performance of trajectory planning methods based on different networks, the root mean square error (RMSE) of the trajectories generated by different methods relative to the optimal trajectory is calculated:

$$Q_{RMSE} = \sqrt{\frac{1}{N_k}\sum_{k=1}^{N_k}(\boldsymbol{x}_k^{O} - \boldsymbol{x}_k^{\mathcal{N}})^2} \tag{21}$$

TABLE IV
RMSE OF TRAJECTORY STATES FOR DIFFERENT METHODS

Method	x_A	y_A	θ_A	v_A	ϑ_A
Proposed	0.012356	0.013895	0.000460	0.011261	0.000214
CNN-LSTM	0.012798	0.035693	0.000864	0.011464	0.000234
LSTM-Attention	0.012608	0.021226	0.001297	0.047074	0.000287
LSTM-RDNN	0.014507	0.051359	0.001515	0.014626	0.000265
GRU	0.013255	0.082367	0.001634	0.030793	0.000261
RDNN	0.012852	0.029931	0.002031	0.015011	0.000443
DNN	0.013385	0.038903	0.002287	0.041138	0.000254

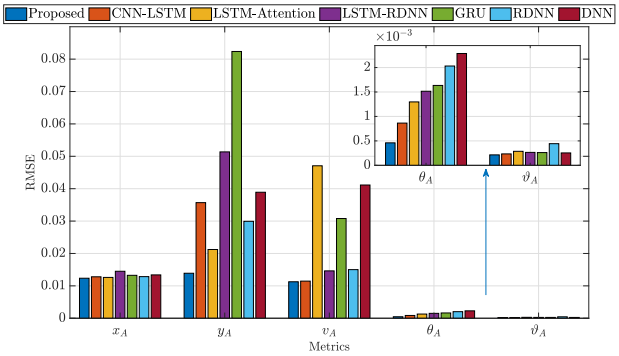

Fig. 12. Visualization of RMSE comparison for different methods.

where N_k denotes the number of points in a trajectory, $\boldsymbol{x}_k^O$ represents the optimal trajectory points, and $\boldsymbol{x}_k^{\mathcal{N}}$ represents the trajectory points planned by the network-based method. RMSE reflects the square root of the difference between the trajectories planned by the network-based methods and the optimal trajectory. A smaller RMSE indicates better performance of the method.

Tab. IV presents the RMSE statistics of the trajectories generated by different network-based methods relative to the optimal trajectory (with 300 trajectories designed for the statistical analysis). Fig. 12 provides a visual comparison of these RMSE statistics. The results clearly show that, compared to other network-based methods, the trajectories planned by the proposed method have a smaller RMSE. This further confirms the optimality of the proposed method in the AGV lane-change trajectory design task compared to other methods.

E. Validation of the Robustness of the Self-Attention Guided CNN-LSTM in Trajectory Planning

To demonstrate the broad applicability and robustness of the real-time trajectory planner based on the self-attention guided CNN-LSTM network designed in this study for addressing the autonomous lane-change problem of AGVs, 300 Monte Carlo experiments are conducted. These experiments involve real-time trajectory planning under various HDV acceleration settings, with the acceleration settings range from Scenario 1: $[0.2, 0.5]$ m/s^2 and Scenario 2: $[-0.3, 0]$ m/s^2. The results of the planned trajectories are shown in Fig. 13, and the corresponding state curves are presented in Fig. 14. In these two scenarios, the acceleration ranges for the HDV are set differently. To achieve a safe lane-change maneuver, the AGV should be positioned behind the HDV after changing the lane in Scenario 1, while it should be positioned in front of the HDV after changing the lane in Scenario 2.

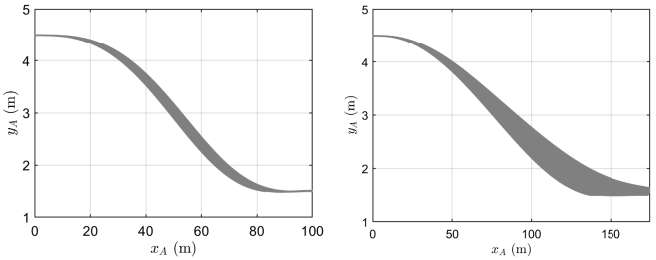

Fig. 13. The trajectories in the two scenarios of the Monte Carlo experiment.

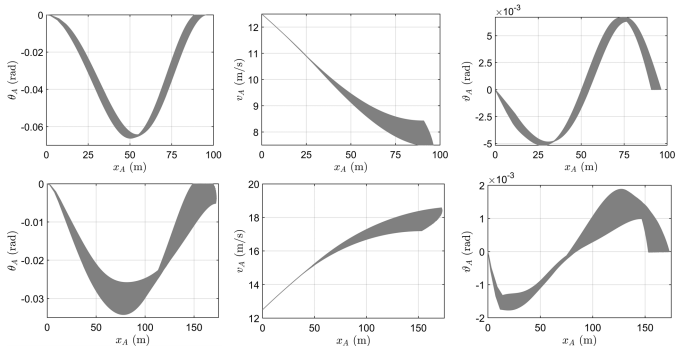

Fig. 14. The trajectory state curves in the two scenarios of the Monte Carlo experiment.

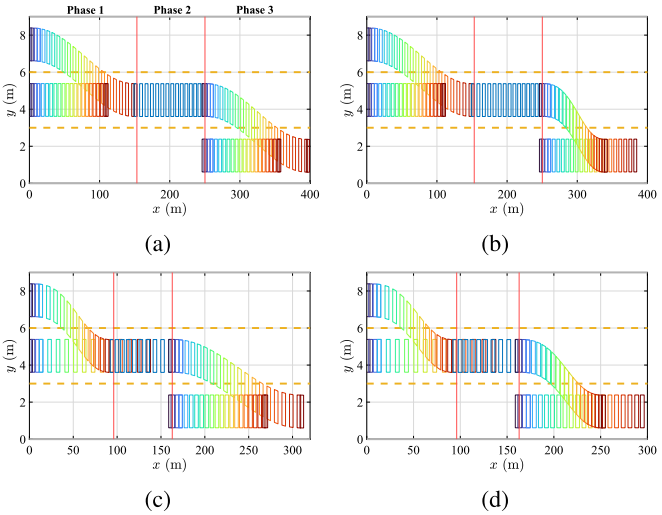

Fig. 15. Trajectory planning results in different three-lane lane-change scenarios.

The Monte Carlo experiment results indicate that the trained online trajectory planner can guide the AGV to decelerate in Scenario 1 and accelerate in Scenario 2, ensuring the design of correct and safe lane-change trajectories without violating state constraints. This demonstrates the effectiveness and robustness of the online trajectory planner in handling AGV lane-change tasks under various conditions.

Moreover, the proposed framework has been extended to more complex lane-change scenarios, specifically trajectory planning in a three-lane environment, with the corresponding planning results shown in Fig. 15. In the three-lane scenario, continuous lane-change may increase the risk of accidents. To enhance safety and meet lane-change conditions, the lane-change process is divided into three stages: Phase 1 (Lane

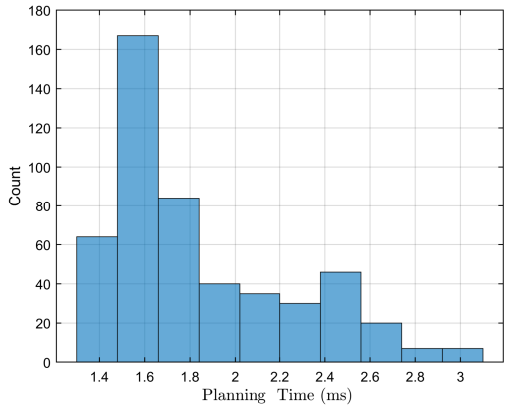

Fig. 16. Statistical chart of the time required for a single inference by the network.

Change Phase 1), Phase 2 (Straight-Driving Phase), and Phase 3 (Lane Change Phase 2). In Figs. 15a, 15b, 15c, 15d, the HDV driving intentions for the first lane-change and second lane-change are -0.2492 m/s^2 and -0.2552 m/s^2, -0.2492 m/s^2 and 0.2090 m/s^2, 0.2090 m/s^2 and -0.2492 m/s^2, and 0.2090 m/s^2 and 0.2150 m/s^2, respectively. In Lane Change Phases 1 and 2, the same color represents the positions of the AGV and HDV at the same time. The results indicate that in various three-lane lane-change scenarios, the proposed framework consistently generates safe and feasible lane-change trajectories for the AGV, demonstrating its robustness and applicability. Furthermore, the application of this framework in three-lane environments can be further extended to multi-lane traffic scenarios to achieve more complex lane-change trajectory planning.

F. Real-Time Analysis of the Self-Attention Guided CNN-LSTM Trajectory Planner

One major advantage of the network-based trajectory planner is its real-time online trajectory planning capability. In this study, we verified the real-time performance of the proposed method through statistical analysis. To this end, the time taken for 500 single inferences using the proposed network is recorded and the corresponding analysis is provided, as shown in Fig. 16. Each network inference process includes data normalization, model inference, data denormalization, and vehicle state integration operations. As illustrated in the figure, the single inference planning time using the proposed network remains within a very small range, with an average time of approximately 1.8 ms. This efficient computation ensures that the trajectory planner can rapidly generate AGV lane-change control commands upon receiving the HMMT system state, thereby meeting the real-time requirements of AGV lane-change tasks.

G. Physical Experiment Results

To further validate the effectiveness and practical application potential of the proposed trajectory planning framework, a physical experiment is conducted in this subsection. The relevant parameters of the vehicles are listed in Tab. V.

TABLE V
PHYSICAL EXPERIMENT PARAMETERS

Parameter	Value/Range	Parameter	Value/Range
d_{safe}	2 m	$AGV-l_w$	0.71 m
$AGV-l_m$	0.21 m	$AGV-l_a$	0.97 m
$AGV-l_f$	0.22 m	$HDV-l_w$	0.73 m
$HDV-l_m$	0.20 m	$HDV-l_a$	1.13 m
$HDV-l_f$	0.20 m	$[x_{\min}, x_{\max}]$	$[0, 10]$ m
$[y_{\min}, y_{\max}]$	$[0, 2]$ m	$[v_{\min}, v_{\max}]$	$[0, 2]$ m/s
$[\theta_{\min}, \theta_{\max}]$	$[-90, 90]$ deg	$[\vartheta_{\min}, \vartheta_{\max}]$	$[-30, 30]$ deg
$[a_{\min}, a_{\max}]$	$[-0.5, 0.5]$ m/s^2	$[c_{\min}, c_{\max}]$	$[-0.6, 0.6]$ rad/(m $\cdot$ s)

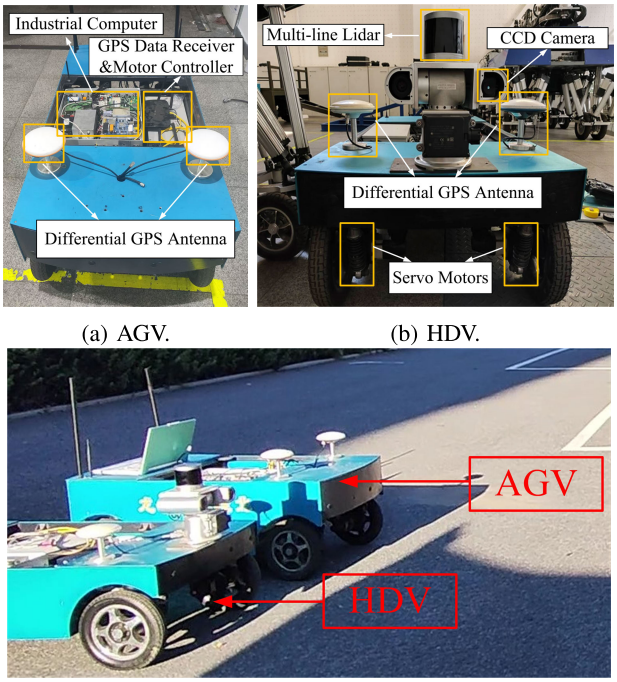

(a) AGV. (b) HDV.

(c) Experimental scenario.

Fig. 17. Experimental platforms and experimental scenario.

Fig. 17c shows the experimental scenario. The AGV and HDV start at positions (0 m, 1.5 m) and (0 m, 0.5 m), respectively. Additionally, $a_H = 0.2$ m/s^2, and it is set that the AGV is positioned in front of the HDV after changing the lane.

The experimental platform, as shown in Fig. 17, consists of two different four-wheel vehicles: one functioning as an AGV and the other as an HDV. Both vehicles are controlled by industrial computers equipped with I7-8500 CPUs and GTX 1660TI GPUs and equipped with 8 Syntron 60CB020C-500000 AC servo MOTPrs for wheel power drive and wheel steering drive. They also use the ML7700 inertial measurement unit and differential GPS with RTK technology, achieving a positioning accuracy of ± 0.8 cm. The onboard industrial computers run the Ubuntu 20.04 operating system and use ROS Noetic as the software development framework.

In the physical experiment, the HDV is set to move in a straight line, consistent with the simulation experiment, while the AGV performed an autonomous lane-change maneuver. During this process, both the AGV and HDV acquire their state information through onboard sensors, collectively forming the HMMT system state. This state information is then fed into the proposed self-attention guided CNN-LSTM trajectory planner

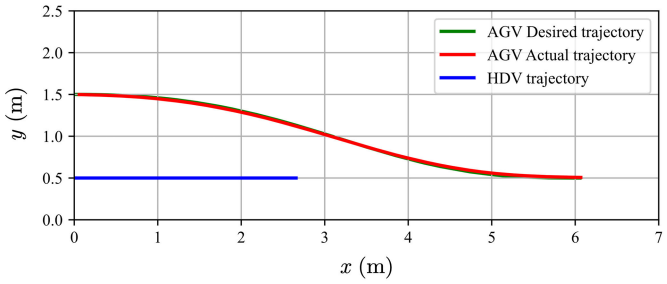

Fig. 18. Trajectory tracking.

to generate planning commands and determine the AGV's next position. The pure pursuit algorithm is subsequently employed for trajectory tracking. The generated trajectory is shown as the green line in Fig. 18. Experimental results demonstrate that the proposed method can generate safe AGV lane-change trajectories in real time, and the resulting trajectories are easy to track, meeting the design objectives. These findings validate the effectiveness of the proposed method and its potential for real-world applications. More details can be found in the video: https://youtu.be/Ri8RL31d7dc.

VI. Discussion

The proposed framework uses IT2PP and FFOA to build a dataset that includes multi-objective optimal control actions for the AGV under various HDV driving intentions, along with the corresponding HMMT system states. The self-attention guided CNN-LSTM is then applied to learn the relationship between the HMMT system states and AGV control actions, facilitating real-time trajectory planning. Due to the use of fitting functions to construct obstacle avoidance constraints, FFOA exhibits lower complexity compared to the obstacle avoidance methods in [22] and [23], thereby enhancing computational efficiency. IT2FPP treats all boundaries in the preference function as IT2FNs, effectively addressing the uncertainty of all boundaries and the fuzzy preferences of multiple DMs, overcoming the limitations of FPP. The self-attention guided CNN-LSTM is specifically designed for time series data, efficiently capturing internal temporal features from multiple perspectives. Therefore, this network demonstrates higher accuracy compared to other neural network-based trajectory planning methods. Furthermore, by incorporating HDV driving intentions during the data construction process, there is no need to infer them when performing real-time trajectory planning for the AGV in the HMMT, further enhancing real-time performance. Simulation and physical experiments, as well as comparative analyses with related works validate the effectiveness of the framework.

However, the current study has certain limitations, as it only considers lane-change tasks with a single HDV in an idealized, noise-free environment. Future research could extend this framework to more complex and realistic driving scenarios of HMMT, including diverse traffic conditions (e.g., varying obstacle distributions, adverse road conditions such as flooded road and road with hail [44]), different types of vehicles (e.g., scenarios involving multiple HDVs and heterogeneous traffic flows), and more complex human driving behaviors. Researchers can fully consider these driving scenarios when constructing datasets and apply the algorithmic framework presented in this study for multi-objective real-time trajectory planning of AGVs. This will further extend the applicability of our framework and evaluate its robustness and adaptability under a wider range of driving conditions.

Additionally, as the level of autonomous driving increases, human intervention will decrease, and AGVs will become more perfect. Due to the superior computational power of computers compared to humans, the higher the level of AGVs, the more efficient our multi-objective real-time trajectory planning model will become. Nevertheless, it should be noted that the deployment of AGVs with intelligent decision-making capabilities should not be constrained by perfectionist standards. Instead, their potential advantages should be realized through continuous optimization. At the same time, human-in-the-loop (HITL) or human-on-the-loop (HOTL) teleoperation capacity of humans can be used to tackle difficult conditions that AGV cannot be managed autonomously. Specifically, in the HITL mode, humans directly participate in decision-making [45], compensating for the limitations of the automation system in complex scenarios. On the other hand, HOTL ensures that human supervision and intervention are available to correct the system at critical moments [46]. Therefore, a HITL or HOTL remote intervention mechanism can be established based on practical needs, addressing the concerns of various stakeholders regarding safety and reliability, and promoting the practical application of intelligent decision-making AGVs.

VII. Conclusion

This study provides a comprehensive and in-depth analysis of the related works in multi-objective real-time trajectory planning for AGVs in HMMT, including HDV driving intention inference, obstacle avoidance constraints, multi-objective trajectory planning, and neural network based trajectory planning. Given the inefficiencies, compatibility issues, and accuracy limitations in existing works, this study proposes a self-attention guided CNN-LSTM based framework to address the multi-objective real-time trajectory planning problem for AGVs in HMMT. In this framework, we introduce IT2PP and FFOA to construct a dataset that encompasses multi-objective optimal control actions for the AGV under different HDV intents, as well as the corresponding HMMT system states. The proposed self-attention guided CNN-LSTM is then utilized to learn the mapping function between the HMMT system states and AGV control actions, enabling real-time trajectory planning. Based on simulation and physical experiment results, along with comparative analyses with related works, the following conclusions can be drawn: (1) The proposed FFOA method effectively addresses AGV obstacle avoidance with lower complexity, enhancing computational efficiency; (2) IT2FPP effectively handles situations where all boundaries of the preference function are uncertain and expresses fuzzy preferences from multiple DMs, overcoming the limitations of FPP; (3) The proposed network can more accurately learn the mapping function between HMMT system states and AGV control actions, resulting in safer trajectory planning; (4) The proposed framework eliminates the need for

HDV driving intention inference in AGV real-time trajectory planning in HMMT, further improving real-time performance; (5) The framework proposed in this study has practical application potential. In conclusion, this study demonstrates the high accuracy, real-time performance, and practical application potential of the proposed framework. The contributions of this study, particularly the method of incorporating HDV driving intentions during dataset construction, thereby eliminating the need to infer them when planning AGV trajectories in real-time, advance technological innovation in AGV trajectory planning and autonomous driving, offering new perspectives and solutions for researchers and engineers in the fields of autonomous driving and intelligent transportation.

REFERENCES

[1] Y. Wiseman, *Autonomous Vehicles*. Hershey, PA, USA: IGI Global, Jul. 2020, pp. 1–11.

[2] J. Fell, "Cars of the future [transport concept cars]," *Eng. Technol.*, vol. 12, no. 2, pp. 48–53, Mar. 2017.

[3] K. Kuru and W. Khan, "A framework for the synergistic integration of fully autonomous ground vehicles with smart city," *IEEE Access*, vol. 9, pp. 923–948, 2021.

[4] Y. Huang, J. Du, Z. Yang, Z. Zhou, L. Zhang, and H. Chen, "A survey on trajectory-prediction methods for autonomous driving," *IEEE Trans. Intell. Vehicles*, vol. 7, no. 3, pp. 652–674, Sep. 2022.

[5] R. van Hoek, J. Ploeg, and H. Nijmeijer, "Cooperative driving of automated vehicles using B-splines for trajectory planning," *IEEE Trans. Intell. Vehicles*, vol. 6, no. 3, pp. 594–604, Sep. 2021.

[6] T. Mercy, R. Van Parys, and G. Pipeleers, "Spline-based motion planning for autonomous guided vehicles in a dynamic environment," *IEEE Trans. Control Syst. Technol.*, vol. 26, no. 6, pp. 2182–2189, Nov. 2018.

[7] L. Ma, J. Xue, K. Kawabata, J. Zhu, C. Ma, and N. Zheng, "Efficient sampling-based motion planning for on-road autonomous driving," *IEEE Trans. Intell. Transp. Syst.*, vol. 16, no. 4, pp. 1961–1976, Aug. 2015.

[8] J. Yin, Z. Hu, Z. P. Mourelatos, D. Gorsich, A. Singh, and S. Tau, "Efficient reliability-based path planning of off-road autonomous ground vehicles through the coupling of surrogate modeling and RRT," *IEEE Trans. Intell. Transp. Syst.*, vol. 24, no. 12, pp. 15035–15050, Dec. 2023.

[9] R. Zhang, R. Chai, S. Chai, Y. Xia, and A. Tsourdos, "Design and practical implementation of a high efficiency two-layer trajectory planning method for AGV," *IEEE Trans. Ind. Electron.*, vol. 71, no. 2, pp. 1811–1822, Feb. 2023.

[10] M. Likhachev and D. Ferguson, "Planning long dynamically feasible maneuvers for autonomous vehicles," *Int. J. Robot. Res.*, vol. 28, no. 8, pp. 933–945, Aug. 2009.

[11] Q. Liu, L. Zhao, Z. Tan, and W. Chen, "Global path planning for autonomous vehicles in off-road environment via an A-star algorithm," *Int. J. Vehicle Auto. Syst.*, vol. 13, no. 4, pp. 330–339, 2017.

[12] B. Li et al., "Optimization-based trajectory planning for autonomous parking with irregularly placed obstacles: A lightweight iterative framework," *IEEE Trans. Intell. Transp. Syst.*, vol. 23, no. 8, pp. 11970–11981, Aug. 2021.

[13] R. Chai et al., "A two phases multiobjective trajectory optimization scheme for multi-UGVs in the sight of the first aid scenario," *IEEE Trans. Cybern.*, vol. 54, no. 9, pp. 5078–5091, Sep. 2024.

[14] T. Qie et al., "An improved model predictive control-based trajectory planning method for automated driving vehicles under uncertainty environments," *IEEE Trans. Intell. Transp. Syst.*, vol. 24, no. 4, pp. 3999–4015, Apr. 2023.

[15] L. Chen, M. Wu, W. Pedrycz, and K. Hirota, "Multi-support vector machine based Dempster-Shafer theory for gesture intention understanding," in *Emotion Recognition and Understanding for Emotional Human-Robot Interaction Systems*. Cham, Switzerland: Springer, 2021, pp. 115–131, doi: 10.1007/978-3-030-61577-2_8.

[16] X. Gao, L. Yan, G. Wang, and C. Gerada, "Hybrid recurrent neural network architecture-based intention recognition for human–robot collaboration," *IEEE Trans. Cybern.*, vol. 53, no. 3, pp. 1578–1586, Mar. 2023.

[17] Z. Yu, D. S. Moirangthem, and M. Lee, "Continuous timescale long-short term memory neural network for human intent understanding," *Frontiers Neurorobot.*, vol. 11, p. 42, Aug. 2017.

[18] J. Lu, S. Hossain, W. Sheng, and H. Bai, "Cooperative driving in mixed traffic of manned and unmanned vehicles based on human driving behavior understanding," in *Proc. IEEE Int. Conf. Robot. Autom. (ICRA)*, May 2023, pp. 3532–3538.

[19] D. Filev, J. Lu, F. Tseng, and K. Prakah-Asante, "Real-time driver characterization during car following using stochastic evolving models," in *Proc. IEEE Int. Conf. Syst., Man, Cybern.*, Oct. 2011, pp. 1031–1036.

[20] Y. Pang, G. Zhang, and H. Xia, "Autonomous driving traffic control based on human-in-the-loop decisions," in *Proc. 33rd Chin. Control Decis. Conf. (CCDC)*, May 2021, pp. 1116–1121.

[21] N.-N. Mei and Z.-J. Wang, "Moving object detection algorithm based on Gaussian mixture model," *Comput. Eng. Design*, vol. 33, no. 8, pp. 3149–3153, 2012.

[22] R. Chai, A. Tsourdos, S. Chai, Y. Xia, A. Savvaris, and C. L. P. Chen, "Multiphase overtaking maneuver planning for autonomous ground vehicles via a desensitized trajectory optimization approach," *IEEE Trans. Ind. Informat.*, vol. 19, no. 1, pp. 74–87, Jan. 2023.

[23] Z. Xing, R. Chai, K. Chen, Y. Xia, and S. Chai, "Online trajectory planning method for autonomous ground vehicles confronting sudden and moving obstacles based on LSTM-attention network," *IEEE Trans. Cybern.*, vol. 55, no. 1, pp. 421–435, Jan. 2025.

[24] P. Zips, M. Böck, and A. Kugi, "Optimisation based path planning for car parking in narrow environments," *Robot. Auto. Syst.*, vol. 79, pp. 1–11, May 2016.

[25] B. Li et al., "Embodied footprints: A safety-guaranteed collision-avoidance model for numerical optimization-based trajectory planning," *IEEE Trans. Intell. Transp. Syst.*, vol. 25, no. 2, pp. 2046–2060, Oct. 2023.

[26] R. Chai, A. Tsourdos, A. Savvaris, S. Chai, and Y. Xia, "Two-stage trajectory optimization for autonomous ground vehicles parking maneuver," *IEEE Trans. Ind. Informat.*, vol. 15, no. 7, pp. 3899–3909, Jul. 2019.

[27] G. Zhang, S. Chai, R. Chai, M. Garcia, and Y. Xia, "Fuzzy goal programming algorithm for multi-objective trajectory optimal parking of autonomous vehicles," *IEEE Trans. Intell. Veh.*, vol. 9, no. 1, pp. 1909–1918, Jan. 2024.

[28] X. Lin, T. Wang, S. Zeng, Z. Chen, and L. Xie, "Autonomous vehicles lane-changing trajectory planning based on hierarchical decoupling," *IEEE Trans. Intell. Transp. Syst.*, vol. 25, no. 12, pp. 20741–20752, Dec. 2024.

[29] R. Chai, A. Savvaris, and A. Tsourdos, "Fuzzy physical programming for space manoeuvre vehicles trajectory optimization based on hp-adaptive pseudospectral method," *Acta Astronautica*, vol. 123, pp. 62–70, Jun. 2016.

[30] R. Chai, A. Savvaris, A. Tsourdos, and Y. Xia, "An interactive fuzzy physical programming for solving multiobjective skip entry problem," *IEEE Trans. Aerosp. Electron. Syst.*, vol. 53, no. 5, pp. 2385–2398, Oct. 2017.

[31] Y.-L. Qi, C.-C. Cai, and P.-Z. Lang, "Mathematical modeling on multi-stage series crushing ratio distribution based on fuzzy physical programming," *J. Coal Sci. Eng.*, vol. 19, no. 2, pp. 262–267, Jun. 2013.

[32] M. Mohammadpour et al., "Energy-efficient motion planning of an autonomous forklift using deep neural networks and kinetic model," *Expert Syst. Appl.*, vol. 237, Mar. 2024, Art. no. 121623.

[33] R. Chai, D. Liu, T. Liu, A. Tsourdos, Y. Xia, and S. Chai, "Deep learning-based trajectory planning and control for autonomous ground vehicle parking maneuver," *IEEE Trans. Autom. Sci. Eng.*, vol. 20, no. 3, pp. 1633–1647, Jul. 2022.

[34] K. Chen, R. Chai, R. Zhang, Z. Xing, Y. Xia, and G. Liu, "A data-driven real-time trajectory planning and control methodology for UGVs using LSTMRDNN," *IEEE/CAA J. Autom. Sinica*, vol. 11, no. 5, pp. 1292–1294, May 2024.

[35] L. Huang, R. Chai, Z. Xing, K. Chen, S. Chai, and Y. Xia, "Real-time trajectory planning for logistical supply transportation using GRU neural networks," in *Proc. 3rd Int. Conf. Auto. Unmanned Syst. (ICAUS)*, Singapore, Y. Qu, M. Gu, Y. Niu, and W. Fu, Eds., Springer, Jan. 2024, pp. 244–254.

[36] B. Li and Z. Shao, "A unified motion planning method for parking an autonomous vehicle in the presence of irregularly placed obstacles," *Knowl.-Based Syst.*, vol. 86, pp. 11–20, Sep. 2015.

[37] B. Sakcak, L. Bascetta, G. Ferretti, and M. Prandini, "An admissible heuristic to improve convergence in kinodynamic planners using motion primitives," *IEEE Control Syst. Lett.*, vol. 4, no. 1, pp. 175–180, Jan. 2020.

[38] P. Khalaf and H. Richter, "Trajectory optimization of robots with regenerative drive systems: Numerical and experimental results," *IEEE Trans. Robot.*, vol. 36, no. 2, pp. 501–516, Apr. 2020.
[39] A. Messac, "Physical programming-effective optimization for computational design," *AIAA J.*, vol. 34, no. 1, pp. 149–158, 1996.
[40] J. Hu, Y. Zhang, X. Chen, and Y. Liu, "Multi-criteria decision making method based on possibility degree of interval type-2 fuzzy number," *Knowl.-Based Syst.*, vol. 43, pp. 21–29, May 2013.
[41] P. Peng, Y. Chen, W. Lin, and J. Z. Wang, "Attention-based CNN–LSTM for high-frequency multiple cryptocurrency trend prediction," *Expert Syst. Appl.*, vol. 237, Mar. 2024, Art. no. 121520.
[42] J. Tang, Y. Li, M. Ding, H. Liu, D. Yang, and X. Wu, "An ionospheric TEC forecasting model based on a CNN-LSTM-attention mechanism neural network," *Remote Sens.*, vol. 14, no. 10, p. 2433, May 2022.
[43] G. Xie, A. Shangguan, R. Fei, W. Ji, W. Ma, and X. Hei, "Motion trajectory prediction based on a CNN-LSTM sequential model," *Sci. China Inf. Sci.*, vol. 63, no. 11, Nov. 2020, Art. no. 212207.
[44] Y. Wiseman, "Real-time monitoring of traffic congestions," in *Proc. IEEE Int. Conf. Electro Inf. Technol. (EIT)*, May 2017, pp. 501–505.
[45] R. Crootof, M. E. Kaminski, W. Price, and I. Nicholson, "Humans in the loop," *Vanderbilt Law Rev.*, vol. 76, no. 2, pp. 429–510, Mar. 2023. [Online]. Available: https://papers.ssrn.com/sol3/papers.cfm?abstract_id=4066781
[46] S. Nahavandi, "Trusted autonomy between humans and robots: Toward human-on-the-loop in robotics and autonomous systems," *IEEE Syst., Man, Cybern., Mag.*, vol. 3, no. 1, pp. 10–17, Jan. 2017.

Gaochang Zhang received the M.S. degree in aeronautical and astronautical science and technology from Dalian University of Technology, Dalian, China, in 2021. He is currently pursuing the Ph.D. degree in control science and engineering with Beijing Institute of Technology, Beijing, China. His research interests are multi-objective optimization and fuzzy control.

Zhida Xing received the B.S. degree in automation from Beijing Institute of Technology, Beijing, China, in 2023, where he is currently pursuing the M.S. degree in control science and engineering with the School of Automation. His primary research interests include trajectory planning and optimization, neural networks, and control science.

Yue Qiu received the master's degree from the School of Automation, Beijing Institute of Technology, in 2024. She is currently with Beijing Dongchezu Technology Company Ltd., doing research on deep learning algorithms, big models of text graphs, and time series data.

Runjiao Bao received the B.Eng. degree from Jilin University, China, in 2023. He is currently pursuing the M.S. degree in control science and engineering with the State Key Laboratory of Intelligent Control and Decision of Complex Systems, School of Automation, Beijing Institute of Technology, China. He is a member of the State Key Laboratory of Intelligent Control and Decision of Complex Systems. His research interests include trajectory planning and control.

Kun Liu (Senior Member, IEEE) received the Ph.D. degree in electrical engineering and systems from Tel Aviv University, Tel Aviv-Yafo, Israel, in 2012. In 2015, he was with the School of Automation, Beijing Institute of Technology, Beijing, China. His current research interests include networked control, game-theoretic control, and security and privacy of cyber-physical systems, with applications in autonomous systems. He serves as an Associate Editor for *IMA Journal of Mathematical Control and Information* and *Journal of Beijing Institute of Technology*. He is a Conference Editorial Board Member of the IEEE Control Systems Society.

Yuanqing Xia (Fellow, IEEE) received the B.S. degree in fundamental mathematics from the Department of Mathematics, Chuzhou University, Chuzhou, China, in 1991, the M.S. degree in fundamental mathematics from Anhui University, Wuhu, China, in 1998, and the Ph.D. degree in control theory and control engineering from Beijing University of Aeronautics and Astronautics, Beijing, China, in 2001. His current research interests are in the fields of networked control systems, robust control and signal processing, active disturbance rejection control, and flight control.

Senchun Chai (Senior Member, IEEE) received the Ph.D. degree in networked control system from the University of South Wales, Pontypridd, U.K., in 2007. He is currently a Professor with the School of Automation, Beijing Institute of Technology. His current research interests focus on flight control systems, networked control systems, embedded systems, and multi-agent control systems.